Interaction of surface acoustic waves with a narrow electron channel in a piezoelectric material

Godfrey Gumbs*
Department of Physics and Astronomy, Hunter College of the City University of New York, 695 Park Avenue, New York, New York 10021

G. R. Aĭzin
Department of Physical Sciences, Kingsborough College of the City University of New York, 2001 Oriental Boulevard, Brooklyn, New York 11235

M. Pepper†
Cavendish Laboratory, University of Cambridge, Madingley Road, Cambridge CB3 0HE, United Kingdom
(Received 23 June 1997; revised manuscript received 2 September 1997)

The interaction between a surface acoustic wave (SAW) of wave number k and frequency ω and a two-dimensional electron gas in a piezoelectric semiconductor can be expressed in terms of the longitudinal conductivity $\sigma_{xx}(k,\omega)$ and an effective electromechanical coupling coefficient. The resulting velocity change and the attenuation of the transmitted SAW intensity are well known. In a recent paper, Simon [Phys. Rev. B **54**, 13 878 (1996)] calculated the fractional energy change $\Delta U/U$ for a SAW interacting with a two-dimensional sheet embedded in a semi-infinite piezoelectric material and obtained a relationship with the results for the attenuation coefficient and the fractional velocity change. In this paper, $\Delta U/U$ is calculated for a narrow channel of width $r_\perp$ $(kr_\perp \ll 1)$ at a distance d below the surface of a slab of piezoelectric material of finite thickness when an elastic wave is launched on the surface. $\Delta U/U$ is given as a closed-form expression in terms of the velocity of the elastic wave, the elastic constants, and the piezoelectric tensor. Numerical results are presented for $\Delta U/U$ as a function of kd for several values of the thickness of a slab of GaAs/Al_xGa_{1-x}As. [S0163-1829(98)09403-X]

I. INTRODUCTION AND BACKGROUND

It is well known that the velocity of a surface acoustic wave (SAW) in piezoelectric crystals can be modified by the electrical conductivity of conductors that are in their vicinity.[1–3] Attenuation of the SAW takes place when there is dissipation in the conductors.[1] Ingebrigtsen[2] and others[3–5] have shown that the fractional velocity change $\Delta v_s/v_s$ and attenuation coefficient K of an acoustic wave of wave vector k that is launched on the surface of a *semi-infinite* piezoelectric material and interacts with a thin (two-dimensional) conducting layer is given by

$$\frac{\Delta v_s}{v_s} - \frac{iK}{k} = \frac{\alpha^2/2}{1 + i\sigma_{xx}(k,\omega)/\sigma_m} = \frac{\Delta U}{U}, \tag{1}$$

where $\sigma_{xx}(k,\omega)$ is the longitudinal conductivity of the two-dimensional (2D) gas and both α and σ_m depend on the material parameters such as an effective dielectric constant, the SAW velocity, and the piezoelectric stress tensor.[6–8] Also, $\Delta U/U$ is the fractional energy change of the SAW, as derived by Simon.[5] Recently, there has been a considerable amount of interest in the interaction of a SAW with a 2DEG in a GaAs/Al_xGa_{1-x}As heterostructure.[5–16] Simon[5] presented a detailed microscopic theory for $\Delta U/U$ when the conducting conditions are changed from a 2D sheet with finite conductivity to the case when the conductivity is infinite. Simon's result for $\Delta U/U$ is for a wave that travels on the surface of a semi-infinite piezoelectric material for which the attenuation is due to a loss of energy through Joule heating of the two-dimensional electron gas (2DEG) embedded within the material. Consequently, the result for $\Delta U/U$ is complex representing the effect of the energy loss and its real and imaginary parts coincide with the fractional velocity change and the attenuation coefficient, respectively, given by Eq. (1). Knäbchen, Levinson, and Entin-Wohlman[9] calculated the absorption of SAW's by a quantum dot. The present paper extends the work of Simon[5] for $\Delta U/U$ of a narrow channel of width $r_\perp$ $(kr_\perp \ll 1)$ of 2DEG in a slab of thickness L when an elastic wave is launched on one of the surfaces. Such a quasi-one-dimensional system has been produced in a GaAs/Al_xGa_{1-x}As 2DEG by means of a split gate.[10,12] A schematic representation of the geometry is shown in Fig. 1. Our results show that the real and imaginary parts of $\Delta U/U$ are also related to the fractional velocity change and the attenuation coefficient of the elastic wave, respectively, when the dispersion law is linear for thin $(kL \ll 1)$ and thick $(kL \gg 1)$ slabs, so that both the phase and group velocities are the same. Our theory is linear, which is valid when the acoustic wave amplitude is small. The attenuation of the SAW in the piezoelectric heterostructure allows experimentalists to study conducting properties of the 2DEG at the operating frequency of the SAW without any contacts being applied to the sample [see Eq. (1)]. This has been exploited to study the transport properties of 2DEG systems in an applied magnetic field in both the low-field limit[12] as well as the quantum Hall regime. Willet *et al.*[15] found evidence of geometric resonances of the cyclotron motion of composite fermions with SAW wavelengths in a 2DEG near $\frac{1}{2}$ filling factor.

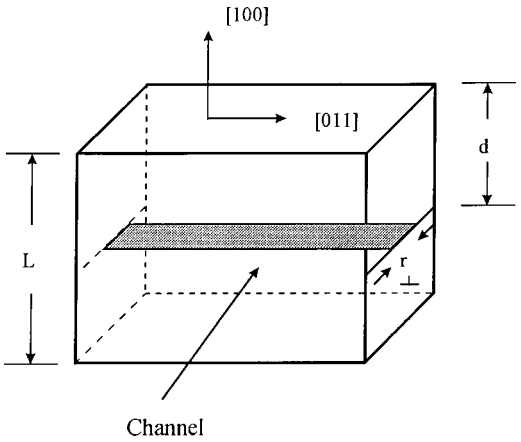

FIG. 1. Schematic of the narrow channel of width $r_\perp$ at a distance d below the surface of a slab of $Al_{0.3}Ga_{0.7}As$ of thickness L. The geometry is relevant for a split gate with Ohmic contacts on the surface where an acoustic wave is launched by transducers.

Another class of problems has been concerned with nonlinear acoustoelectric effects due to the drag of 2D electrons by the SAW.[17] The ac current generated provides a measure of the response of the carriers. It was predicted by Fal'ko, Meshkov, and Iordanski[17] that the current flowing through a channel due to the drag of the electrons by nonequilibrium phonons should be quantized in analogy to conductance quantization. However, in an experiment, Shilton *et al.*[10] showed that the behavior of the acoustoelectric current in a quasi-one-dimensional ballistic channel is qualitatively different from the conductance and there is no quantization of the current as a function of the gate voltage v_g. Specifically, when the acoustoelectric current is plotted as a function of v_g, there are giant oscillations with minima at those gate voltages that show plateaus in the conductance. This was explained by observing that only electrons close to the Fermi energy contribute to the drag current.

An interesting problem that deserves further theoretical investigation concerns the low-field geometric resonances of electron cyclotron modes with the wavelength of a SAW in a high mobility 2DEG. These were clearly seen in experiments by Shilton *et al.*[10] when the acoustoelectric current induced in the 2DEG by the SAW was measured as a function of the magnetic field. The data show that as the magnetic field increases, the acoustoelectric current increases substantially, thereby providing the dependence of the conductivity on the magnetic field. More specifically, the frequency and wave-vector-dependent conductivity could be extracted from these experiments. We would like to determine how the oscillations in the low-field limit are related to the commensurability between the channel width and the cyclotron radius of the electrons at the Fermi energy. Results for the commensurability oscillations in a modulated 2DEG have been reported.[18–22] Recently, Rocke *et al.*[23] have introduced a new form of band-gap engineering by exposing a direct-gap semiconductor quantum well to a moving potential superlattice accompanying a SAW. It is shown that the confinement of photogenerated electron-hole pairs to the 2DEG under the influence of the moving lateral superlattice gives rise to reversible charge separation.

The rest of this paper is organized as follows. In Sec. II, we describe the linear response function formalism and obtain the fractional energy change for a narrow channel ($kr_\perp \ll 1$) in a piezoelectric slab of finite thickness L. This result is expressed in terms of the conductivity of the channel and the electric field potential due to the elastic wave. In Sec. III, we solve the wave equation in a nonpiezoelectric material and use this result to calculate the induced potential in a piezoelectric material in Sec. IV. We also present numerical results for the velocity dependence of the surface wave on the wave vector. Section IV also contains numerical results for the magnitude of the induced electric potential. A brief summary of our results and some concluding remarks are given in Sec. V.

II. GENERAL FORMULATION OF THE PROBLEM

We now describe the formalism that will be used to obtain a generalization of Eq. (1) for a narrow channel within a slab of piezoelectric material of thickness L. The channel is at a distance d below the surface $z=0$ where the SAW is launched. Suppose the SAW propagates along the x direction with the narrow 2D channel of width $r_\perp$ oriented parallel to the x axis. The SAW produces an electric field in the dielectric material described by the electric potential $\varphi^{\rm ext}(k,\omega;z)$, where k is the wave number of the SAW with frequency ω. This potential gives rise to an induced fluctuation charge density $n(k,\omega;y,z)$ in the channel. If the plasma thickness is ignored, then we could set $z=d$ in $\varphi^{\rm ext}$ and n and omit the explicit dependence on the coordinate z wherever it is possible. Our model assumes that the electron motion across the channel in the y direction is restricted by the presence of walls for which the electron distribution in the y direction is approximated by a Gaussian so that the induced charge density $n(k,\omega;y)=\rho_{\rm ind}(k,\omega)\ w(y)$, where $w(y)=\exp(-y^2/2r_\perp^2)/(2\pi r_\perp^2)^{1/2}$ and $r_\perp$ is the channel width. The choice of $w(y)$ is rather arbitrary in doing model calculations but a specific form for it is made for the purpose of simplifying the analytical calculations. A more realistic distribution function could be used if numerical calculations are to be heavily relied upon. The assumption we make is that the density profile in the channel $w(y)$ is a constant throughout the calculation and is never allowed to change even when an external potential is applied. This approximation corresponds to the flow of current in one direction only [see Eq. (10) below].

In linear response theory, the induced charge density $\rho_{\rm ind}(k,\omega)$ is related to the external potential $\varphi^{\rm ext}(k,\omega)$ by

$$\rho_{\rm ind}(k,\omega)=K_{00}(k,\omega)\varphi^{\rm ext}(k,\omega), \tag{2}$$

where $K_{00}(k,\omega)$ is the density-density response function. The induced charge density fluctuation $n(k,\omega;y)$ gives rise to the induced Coulomb potential $\varphi^{\rm ind}(k,\omega;y)$ in the channel. The total potential within the channel is the sum of the external and induced potentials. Following Simon,[5] we can relate charge fluctuations $\rho_{ind}(k,\omega)$ to the total potential $\varphi^{\rm tot}$. For sufficiently narrow channels when $kr_\perp \ll 1$, one can write this relation in the form

$$\rho_{\rm ind}(k,\omega)=\Pi_{00}(k,\omega)\varphi^{\rm tot}(k,\omega), \tag{3}$$

where $\varphi^{\rm tot}(k,\omega)=\varphi^{\rm tot}(k,\omega;y=0)$ and $\Pi_{00}(k,\omega)$ is the polarization function. We then have

$$\varphi^{\rm tot}(k,\omega)=\varphi^{\rm ext}(k,\omega)+v(k)\rho_{\rm ind}(k,\omega), \tag{4}$$

where $v(k)$ is defined by

$$v(k)=\frac{1}{2\pi}\int_{-\infty}^{\infty}dk_y\ \ v(k_{||})f(k_y), \tag{5}$$

with $k_{||}=\sqrt{k^2+k_y^2}$ and

$$f(k_y)\equiv\int_{-\infty}^{\infty}dy\ \ e^{-ik_yy}w(y)$$

$$=e^{-k_y^2r_\perp^2/2}. \tag{6}$$

In Eq. (5), $v(k_{||})$ is the Fourier transform of the Coulomb potential for interacting electrons within the 2D plane embedded in a slab of dielectric material of thickness L with dielectric constant ε, which is assumed isotropic, surrounded by a material with dielectric constant ε_b. The expression for $v(k_{||})$ can be obtained using the method of images and is given by

$$v(k_{||})=\frac{2\pi}{\varepsilon_sk_{||}}\beta(k_{||})\{1+\zeta e^{-2k_{||}d}+\zeta^2e^{-2k_{||}L}+\zeta e^{-2k_{||}(L-d)}\}, \tag{7}$$

where $\varepsilon_s\equiv4\pi\varepsilon_0\varepsilon$ and

$$\zeta\equiv\frac{\varepsilon-\varepsilon_b}{\varepsilon+\varepsilon_b},\quad \beta(k_{||})\equiv\frac{1}{1-\zeta^2e^{-2k_{||}L}}. \tag{8}$$

Equations (5)–(8) jointly yield an explicit result for the Fourier transform of the effective Coulomb potential $v(k)$ in a narrow channel. From Eqs. (2)–(4), it follows that

$$K_{00}^{-1}(k,\omega)=\Pi_{00}^{-1}(k,\omega)-v(k). \tag{9}$$

Our result is a generalization of Simon's result[5] to the case of a narrow channel.

We now proceed to derive an expression for the density-density response function $K_{00}(k,\omega)$ in Eq. (9) in terms of the conductivity $\sigma(k,\omega)$ of the channel. For this, we make use of the continuity equation

$$\nabla\cdot J(\mathbf{r},t)+\frac{\partial n(\mathbf{r},t)}{\partial t}=0, \tag{10}$$

relating the current $J(\mathbf{r},t)$ to the density fluctuations. Taking the Fourier transform of this equation with respect to x and integrating over y, we obtain

$$k^2\sigma(k,\omega)\varphi^{\rm tot}(k,\omega)-i\omega\rho_{\rm ind}(k,\omega)=0, \tag{11}$$

where the relation

$$J(k,\omega)=\sigma(k,\omega)E^{\rm tot}(k,\omega;y=0) \tag{12}$$

between the total current in the channel $J(k,\omega)$ and the total electric field $E^{\rm tot}(k,\omega;y=0)=-ik\varphi^{\rm tot}(k,\omega)$ was used, and $\sigma(k,\omega)$ is the 1D channel conductivity. This approximation is valid for narrow channels when $kr_\perp\ll1$. From Eqs. (3) and (11), it follows that

$$\Pi_{00}(k,\omega)=\frac{k^2\sigma(k,\omega)}{i\omega}. \tag{13}$$

Making use of Eq. (13) in Eq. (9) and setting $\omega=v_sk$ where v_s is the SAW velocity, we obtain

$$K_{00}(k,\omega)=-\frac{1}{v(k)[1-i\sigma_1(k)/\sigma(k,\omega)]}, \tag{14}$$

where

$$\sigma_1(k)=\frac{v_s}{kv(k)}. \tag{15}$$

The next step is to calculate the additional energy induced in the slab due to the interaction of the induced charge density fluctuations in the channel with the electric potential induced by the SAW propagating in the piezoelectric material. The time-averaged expression for this energy per unit surface area is given by

$$\delta\widetilde{U}=\tfrac{1}{2}n\varphi^{\rm ext}\ *. \tag{16}$$

This is a complex energy with its real and imaginary parts directly related to the change of the velocity and dissipation of the SAW.[5] For our geometry, it is more appropriate to calculate the induced energy per unit length along the channel. Integrating Eq. (16) in the y direction and using Eqs. (2) and (14), we obtain

$$\delta\widetilde{U}=-\frac{|\varphi^{\rm ext}|^2}{2v(k)[1-i\sigma_1(k)/\sigma(k,\omega)]}. \tag{17}$$

Following the approach of Ingebrigtsen,[2] one can calculate the energy change with respect to its value for $\sigma=\infty$, which is

$$\delta U=\delta\widetilde{U}(\sigma)-\delta\widetilde{U}(\sigma=\infty)=\frac{|\varphi^{\rm ext}|^2}{2v(k)[1+i\sigma(k,\omega)/\sigma_1(k)]}. \tag{18}$$

In 2D, the fractional energy change $\delta U/U$, where U is the SAW energy per unit surface area of the sample, can be directly related to the change of the SAW velocity and attenuation of the transmitted SAW intensity; see Eq. (1). This interaction between this SAW and 2DEG was considered in detail by Ingebrigtsen[2] and Krasheninnikov and Chaplik.[24] Measurements are usually done in a perpendicular magnetic field where the case $\sigma_{xx}\neq\infty$ corresponds to a measurement in a finite magnetic field whereas $\sigma_{xx}=\infty$ when there is no magnetic field applied to a high-mobility 2D gas.[6–8]

For a 1D channel, the conductivity $\sigma(k,\omega)$ can be varied by changing the width of the channel through the split-gate potential. In this case, the fractional energy change is determined as

$$\frac{\Delta U}{UL_y}\equiv\frac{1}{UL_y}[\,\delta U(\sigma)|_{r_\perp^{(1)}}-\delta U(\sigma)|_{r_\perp^{(2)}}]\ , \tag{19}$$

where L_y is the transverse size of the region where the SAW propagates. If the SAW dispersion is linear, direct calculation of the attenuation coefficient $\Gamma = \mathrm{Re}(J^* E^{\mathrm{tot}}/2I)$, where I is the intensity of the SAW and the velocity change shows that Eq. (1) is still valid with the evident changes $\Delta v_s = v_s|_{r_\perp^{(1)}} - v_s|_{r_\perp^{(2)}}$, $K \to \Delta K = K|_{r_\perp^{(1)}} - K|_{r_\perp^{(2)}}$ and the fractional energy change in Eq. (1) must be replaced by $\Delta U/UL_y$. It is shown below in Sec. III that in general for a slab of finite thickness L the dispersion relation of the elastic wave is nonlinear and the velocity v_s defined above as ω/k is the phase rather than the group velocity of the wave. However, for thin ($kL \ll 1$) and thick ($kL \gg 1$) slabs, the linear dispersion law is restored and both the phase and group velocities are the same. Finally, with all the above mentioned restrictions, Eq. (1) still has a rather broad range of validity. However, although the imaginary part of $\Delta U/U$ gives the attenuation of the wave, the assignment of the real part to be the fractional velocity shift may not be true in general for a nonlinear velocity dispersion. This is a difficult problem that may have some bearing on the experiments for certain SAW wavelengths.

The electric potential φ^{ext} and the energy U in Eqs. (18) and (19) can be obtained by solving the equations describing the propagation of elastic waves in a piezoelectric medium. These equations are[25]

$$c_{ijkl}\frac{\partial^2 u_k}{\partial x_l \partial x_i} + e_{k,ij}\frac{\partial^2 \phi}{\partial x_k \partial x_i} - \rho\frac{\partial^2 u_j}{\partial t^2} = 0, \tag{20a}$$

$$4\pi e_{i,kl}\frac{\partial^2 u_k}{\partial x_l \partial x_i} - \varepsilon_s \nabla^2 \phi = 0, \tag{20b}$$

which must be solved subject to the mechanical boundary conditions and the electrostatic boundary conditions obtained from the continuity of the potential as well as the normal component of the electric displacement vector **D** at the surfaces at $z=0,\ L$, for which

$$D_z = -\varepsilon_s\frac{\partial \phi}{\partial z} + 4\pi e_{z,kl}\frac{\partial u_k}{\partial x_l}, \quad 0<z<L, \tag{21a}$$

$$D_z = -4\pi\epsilon_0\varepsilon_b\frac{\partial \phi}{\partial z}, \quad z<0, \quad z>L. \tag{21b}$$

Mechanical boundary conditions corresponding to the free surfaces at $z=0,\ L$ give us the following equations:

$$c_{izkl}\frac{\partial u_k}{\partial x_l} + e_{k,iz}\frac{\partial \phi}{\partial x_k}\bigg|_{z=0,L} = 0. \tag{22}$$

In this notation, c_{ijkl} is the elastic tensor with $c_{ijkl} = c_{jikl} = c_{ijlk} = c_{klij}$, thereby reducing the number of independent constants to 21,[26] $e_{k,ij}$ is the piezoelectric tensor with $e_{k,ij} = e_{k,ji}$, u_k is the kth component of the lattice displacement, and ρ is the mass density of the medium. Crystals with cubic symmetry such as GaAs and $Al_xGa_{1-x}As$ have only three independent nonzero components of c_{ijkl}, i.e., $c_{11} = c_{xxxx} = c_{yyyy} = c_{zzzz}$, $c_{12} = c_{xxyy} = c_{yyzz} = c_{zzxx}$, and $c_{44} = c_{xyxy} = c_{yzyz} = c_{zxzx}$. All other nonzero components of the elastic tensor are obtained from the symmetry properties given above. A general solution of Eqs. (20a) and (20b) for a semi-infinite medium was given by Campbell and Jones.[25] Here, we obtain the solution of these equations for a slab of finite thickness. In the next section, we solve the wave equation for a nonpiezoelectric medium. The solution for the lattice displacement vector will be employed in Sec. IV to obtain the electric field in Eq. (20) that is produced by this lattice displacement in a piezoelectric material. This solution is equivalent to neglecting the effect the electric field has on the material displacement and is valid to the lowest order in the piezoelectric coupling.

III. ELASTIC WAVES IN A NONPIEZOELECTRIC SLAB OF FINITE THICKNESS

Let us now consider elastic waves in a nonpiezoelectric slab of finite thickness L with cubic crystal symmetry. These waves obey the wave equation (20a) with $e_{k,ij} = 0$ and in this case Eq. (20a) reduces to the well-known equation for elastic waves in cubic crystals.[26–28] The boundary conditions in Eq. (22) yield

$$\frac{\partial u_x}{\partial z} + \frac{\partial u_z}{\partial x}\bigg]_{z=0,\,L} = 0, \tag{23a}$$

$$\frac{\partial u_y}{\partial z} + \frac{\partial u_z}{\partial y}\bigg]_{z=0,\,L} = 0, \tag{23b}$$

$$\left[c_{11}\frac{\partial u_z}{\partial z} + c_{12}\left(\frac{\partial u_x}{\partial x} + \frac{\partial u_y}{\partial y}\right)\right]_{z=0,L} = 0. \tag{23c}$$

We now consider the case when the elastic wave propagates on the (100) surface of a cubic crystal in the [011] direction and for which we take the solution in the following form:

$$\mathbf{u} = \begin{pmatrix} u/\sqrt{2} \\ u/\sqrt{2} \\ u_z \end{pmatrix} e^{-kQz} e^{ik(x+y)/\sqrt{2} - iv_s kt}, \tag{24}$$

corresponding to a wave with wave vector k and frequency $\omega = v_s k$, where the velocity v_s could be wave-vector dependent, as we discuss below. Coordinate axes are chosen along the principal crystallographic axes of the crystal although we assumed the wave to propagate along the x direction in the general formulation of the problem in the preceding section. This form of solution corresponds to the experimental geometry when the launched wave has only one in-plane component of the displacement wave vector along the direction of propagation and u is the amplitude of this displacement.

Substituting Eq. (24) into the wave equation, we obtain

$$(\rho v_s^2 - c_{11}' + c_{44}Q^2)u - i(c_{12}+c_{44})Q\ \ u_z = 0, \quad (25a)$$

$$-i(c_{12}+c_{44})Q\ \ u + (\rho v_s^2 + c_{11}Q^2 - c_{44})u_z = 0, \quad (25b)$$

where $c_{11}' = c_{44} + (c_{11}+c_{12})/2$, for which the determinant of the coefficients in Eq. (25) must be zero for a nontrivial solution. This yields a biquadratic equation for Q with four roots $\pm Q_1$ and $\pm Q_2$, which satisfy

$$Q_1^2 + Q_2^2 = \frac{c_{44}(c_{44}-\rho v_s^2) + c_{11}(c_{11}'-\rho v_s^2) - (c_{12}+c_{44})^2}{c_{11}c_{44}}, \quad (26a)$$

$$Q_1^2 Q_2^2 = \frac{(c_{11}'-\rho v_s^2)(c_{44}-\rho v_s^2)}{c_{11}c_{44}}. \quad (26b)$$

Making use of the results given above, we obtain the general solution of Eq. (25) as

$$\mathbf{u} = \begin{pmatrix} u_1/\sqrt{2} \\ u_1/\sqrt{2} \\ \gamma_1 u_1 \end{pmatrix} e^{-kQ_1 z} e^{ik(x+y)/\sqrt{2} - iv_s kt} + \begin{pmatrix} u_2/\sqrt{2} \\ u_2/\sqrt{2} \\ -\gamma_1 u_2 \end{pmatrix} e^{kQ_1 z} e^{ik(x+y)/\sqrt{2} - iv_s kt}$$
$$+ \begin{pmatrix} u_3/\sqrt{2} \\ u_3/\sqrt{2} \\ \gamma_2 u_3 \end{pmatrix} e^{-kQ_2 z} e^{ik(x+y)/\sqrt{2} - iv_s kt} + \begin{pmatrix} u_4/\sqrt{2} \\ u_4/\sqrt{2} \\ -\gamma_2 u_4 \end{pmatrix} e^{kQ_2 z} e^{ik(x+y)/\sqrt{2} - iv_s kt}, \quad (27)$$

where

$$\gamma_{1,2} = \frac{i(c_{12}+c_{44})Q_{1,2}}{c_{11}Q_{1,2}^2 - c_{44} + \rho v_s^2}, \quad (28)$$

and u_i $(i=1,\ldots,4)$ are arbitrary amplitudes.

Equation (27) and the boundary conditions of Eq. (23) give the following system of equations for u_i after a straightforward but lengthy calculation:

$$\begin{pmatrix} a_{11} & -a_{11} & a_{13} & -a_{13} \\ a_{21} & a_{21} & a_{23} & a_{23} \\ a_{11}e^{-kQ_1L} & -a_{11}e^{kQ_1L} & a_{13}e^{-kQ_2L} & -a_{13}e^{kQ_2L} \\ a_{21}e^{-kQ_1L} & a_{21}e^{kQ_1L} & a_{23}e^{-kQ_2L} & a_{23}e^{kQ_2L} \end{pmatrix} \begin{pmatrix} u_1 \\ u_2 \\ u_3 \\ u_4 \end{pmatrix} = 0, \quad (29)$$

where

$$a_{11} = i\gamma_1 - Q_1, \quad a_{13} = i\gamma_2 - Q_2, \quad (30a)$$

$$a_{21} = c_{12} + i\gamma_1 Q_1 c_{11}, \quad a_{23} = c_{12} + i\gamma_2 Q_2 c_{11}. \quad (30b)$$

The determinant of the coefficient matrix in Eq. (29) must be zero for a nontrivial solution. This condition, in conjunction with Eq. (28) for γ, gives the following result for v_s as a function of kL:

$$[Q_1(c_{11}Q_1^2 + c_{12} + \rho v_s^2)(c_{12}\rho v_s^2 - c_{12}c_{44} - c_{11}c_{44}Q_2^2) + Q_2(c_{11}Q_2^2 + c_{12} + \rho v_s^2)(c_{12}\rho v_s^2 - c_{12}c_{44} - c_{11}c_{44}Q_1^2)]^2 \sinh(kQ_1L)$$
$$\times \sinh(kQ_2L) - 4Q_1Q_2(c_{11}Q_1^2 + c_{12} + \rho v_s^2)(c_{11}Q_2^2 + c_{12} + \rho v_s^2)(c_{12}\rho v_s^2 - c_{12}c_{44} - c_{11}c_{44}Q_1^2)$$
$$\times (c_{12}\rho v_s^2 - c_{12}c_{44} - c_{11}c_{44}Q_2^2)\sinh^2\left(\frac{k(Q_1+Q_2)L}{2}\right) = 0. \quad (31)$$

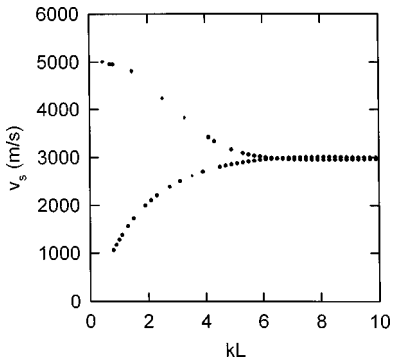

FIG. 2. Plot of the velocity v_s as a function of kL for a slab of $Al_{0.3}Ga_{0.7}As$ of thickness L. The parameters used in the calculation for the elastic stiffness constants and the crystal density for an aluminum concentration $x=0.3$ are given in the text.

When $kL \ll 1$, our calculation shows that in the lowest order of this small parameter, there is only one solution for the velocity, independent of kL and given by

$$v_s^{(l)} = \sqrt{\frac{c_{11}c'_{11}-c_{12}^2}{\rho c_{11}}}, \tag{32}$$

which corresponds to a pure longitudinal wave propagating in a thin crystal sheet. For arbitrary values of kL, Eq. (31), together with Eq. (26), must be solved numerically for v_s, which subsequently yields the dispersion relation $\omega = v_s k$ and the amplitudes u_i from Eq. (29). For $kL \gg 1$, Eq. (31) reduces to a cubic equation derived in Eq. (28) of Ref. 29 for a semi-infinite geometry and [011] propagation of surface waves. In this limiting case, Eqs. (26) and Eq. (31) give one real solution for v_s corresponding to the uncoupled SAW's localized near the top or bottom surface of the slab. Sapriel *et al.*[30] have used Brillouin and Raman scattering to measure v_s of an $Al_xGa_{1-x}As$ alloy as a function of the aluminum concentration. We have solved Eq. (31) for v_s for $Al_xGa_{1-x}As$ for which the elastic stiffness constants are given by the following linear relationships:[31] $c_{11}(x)=11.88+0.14x$, $c_{12}(x)=5.38+0.32x$ and $c_{44}(x)=5.94-0.05x$ in units of $10^{10}N/m^2$. The crystal density for an aluminum concentration x is given by $\rho(x)=(5.36-1.6x)\times 10^3$ kg/m^3. We chose $x=0.3$ and in Fig. 2, we have plotted the solutions v_s as a function of kL. In general, there are two real solutions for v_s as a result of the interaction of the surface elastic modes of the top and bottom surfaces of the slab. However, for small kL, there is only one mode with $v_s=4981$ m/s in agreement with Eq. (32). For large kL, the two modes merge and $v_s=2983$ m/s. Our numerical calculations show that Q_1 is the complex conjugate of Q_2. In Fig. 3, we have plotted the real and the imaginary parts of Q_1 as a function of kL for $Al_xGa_{1-x}As$ with $x=0.3$. Figure 4 is a plot of $\sigma_1(k)$ defined in Eq. (15) as a function of kL for $\varepsilon=(13.18-3.12)x$,[31] $\varepsilon_b=1$, $kd=1.0$, and $r_\perp/L=0.1$. In Fig. 5, we plot $\sigma_1(k)$ as a function of kd, for a variable depth of the 2D layer and fixed kL and $r_\perp/L=0.1$.

Under the conditions $Q_2=Q_1^*$ and, as a consequence, $\gamma_2=-\gamma_1^*$, we have solved Eq. (29) for the eigenvector and

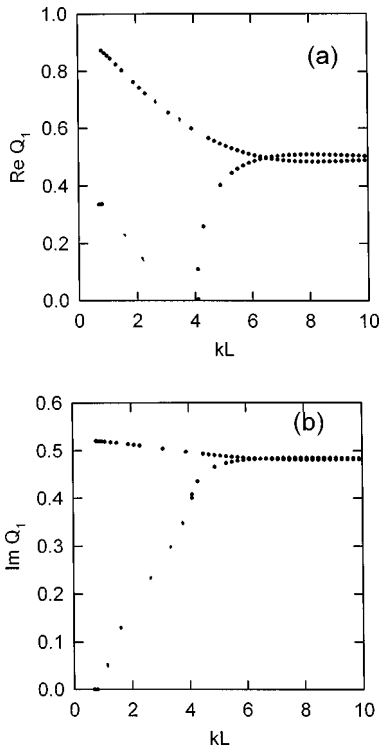

FIG. 3. Plot of the real and imaginary parts of Q_1 as a function of kL for a slab of $Al_{0.3}Ga_{0.7}As$ of thickness L. The parameters used in the calculation for the elastic stiffness constants and the crystal density for an aluminum concentration $x=0.3$ are given in the text.

the results are given by $u_j=(\Delta_j/\Delta)u_1$ for $j=2,\ 3,\ 4$ where Δ_j and Δ are defined as follows:

$$\Delta_2 = 2|a_{11}|^2 a_{21}^* \ [e^{k(Q_1^*-Q_1)L}+e^{-k(Q_1^*+Q_1)L}-e^{-2kQ_1L}-1], \tag{33a}$$

$$\Delta_3 = (|a_{11}|^2 a_{21}-a_{11}^2 a_{21}^*)(e^{kQ_1L}-e^{-kQ_1L})(e^{kQ_1^*L}-e^{-kQ_1L}), \tag{33b}$$

$$\Delta_4 = (a_{11}^2 a_{21}^*+|a_{11}|^2 a_{21})(e^{kQ_1L}-e^{-kQ_1L}) \times (e^{-kQ_1^*L}-e^{-kQ_1L}), \tag{33c}$$

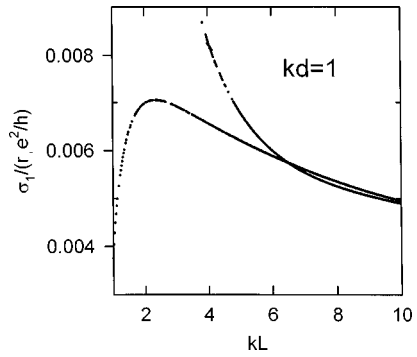

FIG. 4. Plot of $\sigma_1/(r_\perp e^2/h)$ as a function of kL for a slab of $Al_{0.3}Ga_{0.7}As$ of thickness L, $kd=1.0$ and a channel with $r_\perp/L=0.1$. The parameters used in the calculation for the elastic stiffness constants and the crystal density for an aluminum concentration $x=0.3$ are given in the text.

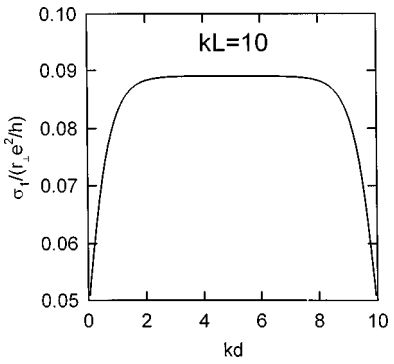

FIG. 5. Plot of $\sigma_1/(r_\perp e^2/h)$ as a function of kd for a slab of $Al_{0.3}Ga_{0.7}As$ of thickness L with $kL=10.0$ and a channel with $r_\perp/L=0.1$. The parameters used in the calculation for the elastic stiffness constants and the crystal density for an aluminum concentration $x=0.3$ are given in the text.

$$\Delta=|a_{11}|^2a_{21}^*[e^{k(Q_1+Q_1^*)L}+e^{-k(Q_1+Q_1^*)L}+e^{k(Q_1-Q_1^*)L}+e^{-k(Q_1-Q_1^*)L}-4]+a_{11}^{*2}a_{21}[e^{k(Q_1-Q_1^*)L}+e^{-k(Q_1-Q_1^*)L}-e^{k(Q_1+Q_1^*)L}-e^{-k(Q_1+Q_1^*)L}]. \tag{34}$$

In general, the energy density associated with the elastic wave can be written as[26,27]

$$E=\tfrac{1}{2}c_{ijkl}u_{ij}u_{kl}^*, \tag{35}$$

where the strain tensor is defined as

$$u_{ij}=\frac{1}{2}\left(\frac{\partial u_i}{\partial x_j}+\frac{\partial u_j}{\partial x_i}\right). \tag{36}$$

From Eqs. (24) and (36), it follows that $u_{xx}=u_{yy}=u_{xy}$ and $u_{yz}=u_{xz}$. Using these results and the symmetry properties of the elastic tensor, Eq. (35) becomes

$$E=2c_{11}'|u_{xx}|^2+\tfrac{1}{2}c_{11}|u_{zz}|^2+2c_{12}\mathrm{Re}(u_{xx}u_{zz}^*)+4c_{44}|u_{xz}|^2. \tag{37}$$

When Eq. (27) is substituted into Eq. (36), the following results for the elastic strain tensor are obtained:

$$u_{xx}=\frac{ik}{\sqrt{2}}u_x, \tag{38a}$$

$$u_{zz}=k\{-\gamma_1Q_1(u_1e^{-kQ_1z}+u_2e^{kQ_1z})+\gamma_1^*Q_1^*(u_3e^{-kQ_1^*z}+u_4e^{kQ_1^*z})\}e^{ik(x+y)/\sqrt{2}-iv_skt}, \tag{38b}$$

$$u_{xz}=\frac{k}{2\sqrt{2}}\{(i\gamma_1-Q_1)(u_1e^{-kQ_1z}-u_2e^{kQ_1z})-(i\gamma_1^*+Q_1^*)\times(u_3e^{-kQ_1^*z}-u_4e^{kQ_1^*z})\}e^{ik(x+y)/\sqrt{2}-iv_skt}. \tag{38c}$$

Substituting Eq. (38) into Eq. (37) and then integrating from $z=0$ to $z=L$, we obtain the energy density per unit surface area as

$$U(k,L)=k|u_1|^2\mathrm{Re}\mathcal{J}(kL), \tag{39}$$

where $\mathcal{J}(kL)$ is given in the Appendix. For a semi-infinite slab, direct calculation shows that

$$\lim_{L\to\infty}\frac{\Delta_2}{\Delta},\quad \frac{\Delta_4}{\Delta}=0,\quad \lim_{L\to\infty}\frac{\Delta_3}{\Delta}=e^{2i\vartheta},\quad e^{2i\vartheta}=-\frac{Q_1-i\gamma_1}{Q_1^*+i\gamma_1^*} \tag{40}$$

and $U(k,L)$ in Eq. (39) reduces to the expression for U given by Simon.[5]

Combining Eqs. (17), (19), and (39), we obtain the fractional energy change in a narrow channel as

$$\frac{\Delta U}{U(k,L)L_y}=\frac{\alpha^2/2}{L_y}\left\{\left.\frac{1}{1+i\sigma(k)/\sigma_1(k,\omega)}\right|_{r_\perp^{(1)}}-\left.\frac{1}{1+i\sigma(k)/\sigma_1(k,\omega)}\right|_{r_\perp^{(2)}}\right., \tag{41}$$

where

$$\frac{\alpha^2}{2}=\frac{|\varphi^{\mathrm{ext}}|^2}{2v(k)k|u_1|^2\mathrm{Re}\,\mathcal{J}(kL)}. \tag{42}$$

In the following section, we calculate the potential φ^{ext} due to an elastic wave launched on the surface of a piezoelectric material.

IV. THE PIEZOELECTRIC EFFECT IN A SLAB OF FINITE THICKNESS

For a piezoelectric medium, the electromagnetic and elastic solutions are coupled, as seen from Eqs. (20). For a cubic crystal, the piezoelectric tensor has only one nonzero independent element given by $e_{x,yz}=e_{y,xz}=e_{z,xy}\equiv e_{14}$ as well as those elements obtained by interchanging the second and third subscripts.[26] We now solve Eq. (20) when the piezoelectric coupling is small, for which the potential in Eq. (20) may be solved using perturbation theory, i.e., we solve for ϕ in Eq. (20b) by making use of the result for the displacement vector obtained by solving Eq. (20a) when the piezoelectric tensor is neglected. In this approximation, the potential is a solution of

$$\nabla^2\phi=\begin{cases}\dfrac{8\pi e_{14}}{\varepsilon_s}\left(2\dfrac{\partial^2u_x}{\partial x\partial z}+\dfrac{\partial^2u_z}{\partial x^2}\right), & 0<z<L\\ 0, & z<0,\quad z>L,\end{cases} \tag{43}$$

where the displacement vector is given by Eqs. (27) and (33). A straightforward calculation shows that $\phi(\mathbf{r},t)=\Phi(z)e^{ik(x+y)/\sqrt{2}-iv_skt}$, where Φ satisfies the equation

$$\varepsilon_s\frac{d^2\Phi}{dz^2}-\varepsilon_s k^2\Phi=4\pi i e_{14}ku_1\left\{2\left[-kQ_1\left(e^{-kQ_1z}-\frac{\Delta_2}{\Delta}e^{kQ_1z}\right)-kQ_1^*\left(\frac{\Delta_3}{\Delta}e^{-kQ_1^*z}-\frac{\Delta_4}{\Delta}e^{kQ_1^*z}\right)\right]\right.$$
$$\left.+ik\left[\gamma_1\left(e^{-kQ_1z}-\frac{\Delta_2}{\Delta}e^{kQ_1z}\right)-\gamma_1^*\left(\frac{\Delta_3}{\Delta}e^{-kQ_1^*z}-\frac{\Delta_4}{\Delta}e^{kQ_1^*z}\right)\right]\right\}. \tag{44}$$

This equation has the particular solution

$$\Phi_p(z)=\frac{4\pi i e_{14}u_1}{\varepsilon_s}\left[C\left(e^{-kQ_1z}-\frac{\Delta_2}{\Delta}e^{kQ_1z}\right)\right.$$
$$\left.+C^*\left(\frac{\Delta_3}{\Delta}e^{-kQ_1^*z}-\frac{\Delta_4}{\Delta}e^{kQ_1^*z}\right)\right], \tag{45}$$

where

$$C\equiv\frac{i\gamma_1-2Q_1}{Q_1^2-1}. \tag{46}$$

Therefore, the general solution for the slab of thickness L is

$$\Phi(z)=\begin{cases}\Phi_p(z)+B_1e^{kz}+B_2e^{-kz}, & 0\leqslant z\leqslant L\\ B_3e^{kz}, & z\leqslant 0\\ B_4e^{-kz}, & z\geqslant L\end{cases}. \tag{47}$$

The continuity conditions of the potential and the normal component of the displacement vector at the surfaces $z=0,\ L$ together give the coefficients in Eq. (47). Since we are interested in the potential within the film, we only present our results for B_1 and B_2. Our calculations show that

$$B_1=\frac{4\pi i e_{14}u_1}{\varepsilon_s}\frac{C_1(\varepsilon_b-\varepsilon)e^{-kL}-C_2(\varepsilon_b+\varepsilon)}{(\varepsilon_b-\varepsilon)^2e^{-kL}-(\varepsilon_b+\varepsilon)^2e^{kL}}$$
$$\equiv\frac{4\pi i e_{14}u_1}{\varepsilon_s}\widetilde{B}_1, \tag{48a}$$

$$B_2=\frac{4\pi i e_{14}u_1}{\varepsilon_s}\frac{C_2(\varepsilon_b-\varepsilon)-C_1(\varepsilon_b+\varepsilon)e^{kL}}{(\varepsilon_b-\varepsilon)^2e^{-kL}-(\varepsilon_b+\varepsilon)^2e^{kL}}\equiv\frac{4\pi i e_{14}u_1}{\varepsilon_s}\widetilde{B}_2 \tag{48b}$$

where

$$C_1=-\left\{[\varepsilon+(\varepsilon_b+\varepsilon Q_1)C]+[\varepsilon+(\varepsilon Q_1-\varepsilon_b)C]\frac{\Delta_2}{\Delta}\right.$$
$$\left.+[\varepsilon+(\varepsilon Q_1^*+\varepsilon_b)C^*]\frac{\Delta_3}{\Delta}+[\varepsilon+(\varepsilon Q_1^*-\varepsilon_b)C^*]\frac{\Delta_4}{\Delta}\right\}, \tag{49a}$$

$$C_2=\left\{[\varepsilon+(\varepsilon Q_1-\varepsilon_b)C]e^{-kQ_1L}+[\varepsilon+(\varepsilon Q_1+\varepsilon_b)C]\right.$$
$$\times\frac{\Delta_2}{\Delta}e^{kQ_1L}+[\varepsilon+(\varepsilon Q_1^*-\varepsilon_b)C^*]\frac{\Delta_3}{\Delta}e^{-kQ_1^*L}+[\varepsilon$$
$$\left.+(\varepsilon Q_1^*+\varepsilon_b)C^*]\frac{\Delta_4}{\Delta}e^{kQ_1^*L}\right\}. \tag{49b}$$

In the limit $kL\gg 1$, making use of Eq. (40) in Eqs. (45)–(49) yields φ^{ext} derived by Simon[5] for a semi-infinite slab. The potential in Eq. (47) yields

$$\varphi^{\text{ext}}=\Phi(d)=\frac{4\pi i e_{14}u_1}{\varepsilon_s}F(kd), \tag{50}$$

where

$$F(kd)=Ce^{-kQ_1d}-\frac{\Delta_2}{\Delta}Ce^{kQ_1d}+\frac{\Delta_3}{\Delta}C^*e^{-kQ_1^*d}$$
$$-\frac{\Delta_4}{\Delta}C^*e^{kQ_1^*d}+\widetilde{B}_1e^{kd}+\widetilde{B}_2e^{-kd}. \tag{51}$$

Substituting Eq. (50) into Eq. (42)

$$\frac{\alpha^2}{2}=\frac{4\pi e_{14}^2}{2v(k)k\varepsilon_s^2\text{Re}\mathcal{J}(kL)}|F(kd)|^2. \tag{52}$$

We now present numerical results for $\alpha^2/2$, which determines the fractional energy change for a narrow channel embedded at a distance d below the surface on which the SAW is launched. In our calculations, we use the piezoelectric constant $e_{14}=-0.16-0.065x$ (C/m^2) for $Al_xGa_{1-x}As$.[31] The results in Fig. 6 show that when $\alpha^2/2L$ is plotted as a function of kd, the plots are very much dependent on the value chosen for kL and $r_\perp$. For $kL=5$, there are two real eigenvalue solutions for the velocity and for which we have plotted the corresponding values of $\alpha^2/2$ in Fig. 6(a). In Fig. 6(b), we set $kL=10$ for which the two surfaces at $z=0$ and $z=L$ are still coupled causing the increase in $\alpha^2/2$ as the surface at $z=L$ is approached. In general, the results for $\alpha^2/2$ for the 2DEG embedded below the surface are not exponential as obtained in other calculations for the half-space geometry ($kL\gg 1$).[5,32] Figure 6(c) is a plot for $kL=50$ when the two surfaces are completely decoupled. The value of $\alpha^2/2L$ is larger for thin films than for thick films. From the combined data in Figs. 1–6, we could now obtain the fractional energy change of the SAW due to the interaction with a narrow channel within a slab of piezoelectric material.

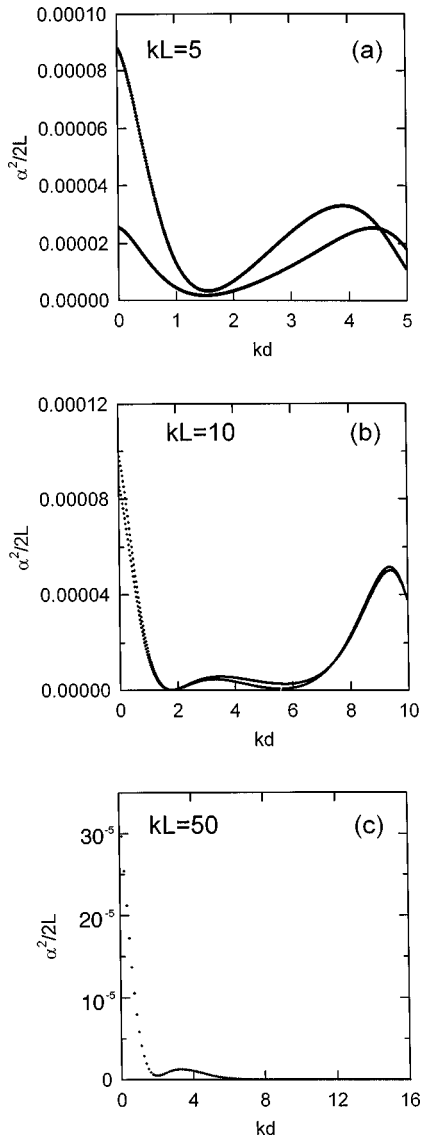

FIG. 6. $\alpha^2/2L$ is plotted as a function of kd for $r_\perp/L=0.1$ and a fixed value of kL chosen as (a) 5, (b) 10, and (c) 50. The parameters used in the calculation for the piezoelectric constants, the elastic stiffness constants, and the crystal density for an aluminum concentration $x=0.3$ are given in the text.

V. SUMMARY AND CONCLUDING REMARKS

In this paper, we have formulated a theory for the fractional energy change $\Delta U/UL_y$ for an elastic wave launched on the surface of a piezoelectric quantum well structure that contains a narrow channel of width $r_\perp$ at a distance d below the surface. Free surface boundary conditions are used in these calculations. The dependence of $\Delta U/U$ on the wave vector k and the 1D channel conductivity $\sigma(k,\omega)$ is obtained. The channel can be realized experimentally in a GaAs/Al_xGa_{1-x}As 2DEG by means of a split gate. When the wave number and the thickness L are such that the two surfaces are coupled then two real solutions for the surface wave velocity are obtained. When the dispersion relation is linear for a thin film ($kL\ll 1$) or a thick film ($kL\gg 1$), the real and imaginary parts of $\Delta U/U$ are related to the velocity change and the attenuation coefficient, respectively. The result for $\Delta U/U$ is given as a closed-form expression in terms of the velocity of the SAW, the elastic constants and the piezoelectric tensor by solving the set of coupled equations for the lattice and electric displacement vectors in the [011] direction on the (100) surface of a cubic crystal. We show that the fractional energy change depends on the parameters $\alpha^2/2$ and σ_1, which are related to the channel conductivity and material characteristics. Numerical results are presented for the velocity of the SAW for $Al_xGa_{1-x}As$ as a function of the thickness of the slab as well as σ_1 as functions of kd and kL. We also compute $\alpha^2/2$ as a function of kd for several values of the thickness of a slab of GaAs/Al_xGa_{1-x}As.

In conclusion, we note that split metal gates are used to produce a narrow conducting channel within a 2DEG. Evidently, the piezoelectric field will be screened by the metallized surface. However, our calculations do not include the effects of screening by the metal gate on the interactions between the electrons within the channel and the launched elastic wave.[7] One method that could be used to reduce the effect of screening is to increase the spatial separation between the gate and the surface where the wave is launched by depositing a relatively thick insulating layer on the surface.[7] Recently, this technique was successfully used by Rocke *et al.*[8] These authors observed the interaction between SAW's and a high-mobility 2DEG in gated GaAs/Al_xGa_{1-x}As heterojunctions and were able to control the carrier density in the 2D gas using gate electrodes.

ACKNOWLEDGMENTS

The authors acknowledge the support in part from the National Science Foundation Grant No. INT-9402741 (U.S. - U.K. Collaborative Grant) and the City University of New York PSC-CUNY Grant No. 664279.

APPENDIX

In this appendix, we give the explicit form for the function $\mathcal{J}(kL)$ in Eq. (39). For convenience of notation, we introduce the function $G(Q,kL)$ defined by

$$G(Q)=\frac{1}{Q}[1-e^{-kQL}]. \tag{A1}$$

In the results presented below, Δ_j for $j=2,\ 3,\ 4$ and Δ are defined in Eqs. (33) and (34). Our calculations show that

$$\begin{aligned}\mathcal{J}(kL)=\frac{1}{|\Delta|^2}\{&A_1[(|\Delta|^2+|\Delta_3|^2)G(Q_1+Q_1^*)\\&+(|\Delta_2|^2+|\Delta_4|^2)G(-Q_1-Q_1^*)]+A_2(\Delta^*\Delta_2\\&+\Delta_3\Delta_4^*)G(Q_1^*-Q_1)+A_3[\Delta\Delta_3^*G(2Q_1)\\&+\Delta_2\Delta_4^*G(-2Q_1)]+A_4(\Delta\Delta_4^*+\Delta_2\Delta_3^*)G(0)\},\end{aligned} \tag{A2}$$

where

$$A_1\equiv\frac{c_{11}'}{2}+\frac{c_{11}}{2}|\gamma_1Q_1|^2+ic_{12}\gamma_1Q_1+\frac{c_{44}}{2}|i\gamma_1-Q_1|^2, \tag{A3}$$

$$A_2 \equiv c_{11}' + c_{11}|\gamma_1 Q_1|^2 + ic_{12}(\gamma_1 Q_1 - \gamma_1^* Q_1^*) - c_{44}|i\gamma_1 - Q_1|^2, \quad \text{(A4)}$$

$$A_3 \equiv c_{11}' - c_{11}\gamma_1^2 Q_1^2 + 2ic_{12}\gamma_1 Q_1 + c_{44}(i\gamma_1 - Q_1)^2, \quad \text{(A5)}$$

$$A_4 \equiv A_3 - 2c_{44}(i\gamma_1 - Q_1)^2. \quad \text{(A6)}$$

The results in Eqs. (A1)–(A6) are used in the calculation of the relative change in energy for the wave launched on the surface of a slab of thickness L.

*Also at The Graduate School and University Center of the City University of New York, 33 West 42 Street, New York, NY 10036.

†Also at Toshiba Cambridge Research Center, 260 Cambridge Science Park, Milton Road, Cambridge CB4 4WE, U.K.

[1] A. R. Hutson and D. L. White, J. Appl. Phys. **33**, 40 (1962).

[2] K. A. Ingebrigtsen, J. Appl. Phys. **40**, 2681 (1969); **41**, 454 (1970).

[3] P. Bierbaum, Appl. Phys. Lett. **21**, 595 (1972).

[4] A. L. Efros and Y. M. Galperin, Phys. Rev. Lett. **64**, 1959 (1990).

[5] S. H. Simon, Phys. Rev. B **54**, 13 878 (1996).

[6] A. Wixforth, J. P. Kotthaus, and G. Weimann, Phys. Rev. B **56**, 2104 (1986).

[7] A. Wixforth, J. Scriba, M. Wassermier, J. P. Kotthaus, G. Weimann, and W. Schlapp, Phys. Rev. B **40**, 7874 (1989).

[8] C. Rocke, S. Manus, A. Wixforth, M. Sundaram, J. H. English, and A. C. Gossard, Appl. Phys. Lett. **65**, 2422 (1994).

[9] A. Knäbchen, Y. B. Levinson, and O. Entin-Wohlman, Phys. Rev. B **55**, 5325 (1997).

[10] J. M. Shilton, D. R. Mace, V. I. Talyanskii, Y. Galperin, M. Y. Simmons, M. Pepper, and D. A. Ritchie, J. Phys.: Condens. Matter **8**, L337 (1996).

[11] J. M. Shilton, D. R. Mace, V. I. Talyanskii, M. Y. Simmons, M. Pepper, A. C. Churchill, and D. A. Ritchie, J. Phys.: Condens. Matter **7**, 7675 (1995).

[12] J. M. Shilton, D. R. Mace, V. I. Talyanskii, M. Pepper, M. Y. Simmons, A. C. Churchill, and D. A. Ritchie, Phys. Rev. B **51**, 14 770 (1995).

[13] A. Esslinger, R. W. Winkler, C. Rocke, A. Wixforth, J. P. Kotthaus, H. Nickel, W. Schlapp, and R. Losch, Surf. Sci. **305**, 83 (1994).

[14] A. Esslinger, A. Wixforth, R. W. Winkler, J. P. Kotthaus, H. Nickel, W. Schlapp, and R. Losch, Solid State Commun. **84**, 939 (1992).

[15] R. L. Willett, R. R. Ruel, K. W. West, and L. N. Pfeiffer, Phys. Rev. Lett. **71**, 3846 (1993).

[16] R. L. Willett, M. A. Paalanen, R. R. Ruel, K. W. West, L. N. Pfeiffer, and D. J. Bishop, Phys. Rev. Lett. **65**, 112 (1990).

[17] V. I. Fal'ko, S. V. Meshkov, and S. V. Iordanskii, Phys. Rev. B **47**, 9910 (1993).

[18] D. Weiss, K. von Klitzing, K. Ploog, and G. Weimann, Europhys. Lett. **8**, 179 (1989); also in *High Magnetic Fields in Semiconductor Physics II*, Springer Series in Solid State Sciences Vol. 87, edited by G. Landwehr (Springer-Verlag, Berlin, 1989), p. 357.

[19] R. R. Gerhardts, D. Weiss, and K. von Klitzing, Phys. Rev. Lett. **62**, 1173 (1989).

[20] R. W. Winkler, J. P. Kotthaus, and K. Ploog, Phys. Rev. Lett. **62**, 1177 (1989).

[21] C. G. Smith, M. Pepper, R. Newbury, H. Ahmed, D. G. Hasko, D. C. Peacock, J. E. F. Frost, D. A. Ritchie, G. A. C. Jones, and G. Hill, J. Phys.: Condens. Matter **2**, 3405 (1990).

[22] K. Ensslin and P. M. Petroff, Phys. Rev. B **41**, 12 307 (1990).

[23] C. Rocke, S. Zimmermann, J. P. Kotthaus, G. Böhm, and G. Weimann, Phys. Rev. Lett. **78**, 4099 (1997).

[24] M. V. Krasheninnikov and A. V. Chaplik, Sov. Phys. JETP **48**, 960 (1978); **49**, 921 (1979).

[25] J. J. Campbell and W. R. Jones, IEEE Trans. Sonics Ultrason. **15**, 209 (1968).

[26] B. A. Auld, *Acoustic Fields and Waves in Solids*, Vol. 1 (Wiley, New York, 1973), p. 59.

[27] L. D. Landau and E. M. Lifshitz, *Theory of Elasticity*, 2nd ed. (Pergamon, New York, 1986).

[28] D. K. Ferry, *Semiconductors* (MacMillan, New York, 1991), p. 86.

[29] R. Stonely, Proc. R. Soc. London, Ser. A **232**, 447 (1955).

[30] J. Sapriel, J. C. Michel, J. C. Tolédano, R. Vacher, J. Kervarec, and A. Regreny, Phys. Rev. B **28**, 2007 (1983).

[31] S. Adachi, J. Appl. Phys. **58**, R1 (1985).

[32] R. L. Miller, C. E. Nothnick, and D. S. Bailey, *Acoustic Charge Transport: Device Technology and Applications* (Artec House, Boston, 1992), p. 147.